Volume 1 | Number 1 | Jan 2013 | Pages 1–100

Nanoscale

www.rsc.org/nanoscale

ROYAL SOCIETY OF CHEMISTRY

ROYAL SOCIETY OF CHEMISTRY

www.rsc.org/nanoscale

Nanoscale

ARTICLE

Ultrastable polyethyleneimine-stabilized gold nanoparticles modified with polyethylene glycol for blood pool, lymph node and tumor CT imaging

Yongxing Zhang[a‡], Shihui Wen[b‡], Lingzhou Zhao[c‡], Du Li[d‡], Changcun Liu[c], Wenbin Jiang[a], Xiang Gao[a], Wentao Gu[a], Nan Ma[e], Jinhua Zhao[c]*, Xiangyang Shi[b,d]*, Qinghua Zhao[a]*

Development of new long-circulating contrast agents for computed tomography (CT) imaging of different biological systems still remains a great challenge. Here, we report the design and synthesis of branched polyethyleneimine (PEI)-stabilized gold nanoparticles (Au PSNPs) modified with polyethylene glycol (PEG) for blood pool, lymph node, and tumor CT imaging. In this study, thiolated PEI was first synthesized and used as a stabilizing agent to form AuNPs. The formed Au PSNPs were then grafted with PEG monomethyl ether *via* PEI amine-enabled conjugation chemistry, followed by acetylation of the remaining PEI surface amines. The formed PEGylated Au PSNPs were characterized *via* different methods. We show that the PEGylated Au PSNPs with Au core size of 5.1 nm have a relatively long half-decay time (7.8 h), display better X-ray attenuation property than conventionally used iodine-based CT contrast agents (e.g., Omnipaque), and are hemocompatible and cytocompatible in a given concentration range. These properties of the Au PSNPs afford their uses as a contrast agent for effective CT imagingof blood pool and major organs of rats, lymph node of rabbits, and xenografted tumor model of mice. Importantly, the PEGylated Au PSNPs could be excreted out of the body with time and also showed excellent *in vivo* stability. These findings suggest that the formed PEGylated Au PSNPs may be used as a promising contrast agent for CT imaging of different biological systems.

Introduction

X-ray computed tomography (CT) has been and will continue to be one of the most widely used tools in clinical non-invasive diagnosis due to its cost effectiveness, high density and spatial resolution, deep tissue penetration capability, as well as facile three dimensional reconstruction.[1-4] Alongside the improvement in terms of the instruments, high quality CT imaging is strongly determined by the development of contrast agents, which can effectively enhance the contrast effect for more accurate clinical diagnosis.[1, 4] Unfortunately, conventional iodine-based small molecular contrast agents suffer severe problems of short imaging time, non-specificity, as well as renal toxicity at a relatively high concentration,[5, 6]

[a.] *Department of Orthopaedics, Shanghai Bone Tumor Institute, Shanghai General Hospital, School of Medicine, Shanghai Jiaotong University, Shanghai 200080, People's Republic of China.Email: sawboneszhao@163.com*
[b.] *College of Chemistry, Chemical Engineering and Biotechnology, Donghua University, Shanghai 201620, People's Republic of China.Email: xshi@dhu.edu.cn*
[c.] *Department of Nuclear Medicine, Shanghai General Hospital, School of Medicine, Shanghai Jiaotong University, Shanghai 200080, People's Republic of China.Email: zhaojinhua1963@126.com*
[d.] *State Key Laboratory for Modification of Chemical Fibers and Polymer Materials, College of Materials Science and Engineering, Donghua University, Shanghai 201620, People's Republic of China.*
[e.] *Department of cardiac surgery, University of Rostock, 18055, Germany*
†Electronic Supplementary Information (ESI) available: Additional experimental results. See DOI: 10.1039/x0xx00000x.
‡These authors contributed equally to this work.

limiting the acquisition of the high resolution CT images of the interest site.[5, 7]

With the advantage of nanotechnology, nanoparticulate CT contrast agents have been successfully developed to overcome the drawbacks of small molecular irodinated CT contrast agents.[4, 8, 9] The nanosystems include polymeric particles,[6] nanosuspensions,[10] liposomes,[11, 12] micelles,[13] and inorganic nanospheres.[4, 5, 14-16] Among various compositions, gold nanoparticles (AuNPs) have been proven to be an ideal radiopaque nanoparticulate contrast agent since the first exploitation of AuNPs for X-ray imaging by Hainfeld and his team in 2004.[17, 18] This is because Au has a high atomic number than iodine, and AuNPs have a prolonged blood circulation time and excellent biocompatibility.[18] Moreover, the relative ease of synthesis and control over their size, and ease of surface modification with desired functional groups make them versatile in biomedical applications.[19, 20] However, their further commercial process and clinical applications has often been hampered by their colloidal instability, expensive polymeric carriers, as well as difficulty to be scaled up for mass production. Therefore, development of a facile strategy to form AuNPs-based CT contrast agent for biomedical imaging still remains a great challenge.

Branched polyethyleneimine (PEI) has been widely utilized as the template or stabilizer to synthesize various inorganic NPs due to its cost-effectiveness and wide availability.[21-26] With the PEI amine-enabled conjugation chemistry, biological

ligand molecules can be modified onto the particle surface for targeted drug and gene delivery application,[27-29] and the amines can also be neutralized to reduce the cytotoxicity of the particles.[30-32] In our previous works, we have shown that poly(amidoamine) (PAMAM) dendrimer- or PEI-entrapped AuNPs could be synthesized using PEGylated PAMAM dendrimer or PEI as a template for enhanced blood pool and tumor CTimaging.[2, 33] However, these previous works only report the Au NPs stabilized with the amine group of PAMAM or PEI, which suffer from the issues of colloidal stability in case of high gold loading. For sensitive CT imaging, it is essential to load more Au content at a given amount of PEI with high stability.[34] It is known that thiolated PEI is able to effectively stabilize AuNPs *via* the formation of stable Au-S bond,[35] and thiolated PEI-stabilized Au NPs have been used for effective gene delivery applications.[36-38] These prior studies lead us to hypothesize that thiolated PEI may be used as an effective stabilizer to generate stable PEI-stabilized Au NPs (Au PSNPs) with good stability for CT imaging of different biological systems.

In this present study, Au PSNPs with ultrastability and improved Au composition (Au/PEI molar ratio) were designed and synthesized for CT imaging applications (Scheme 1a). Branched PEI was firstly modified with mercaptoacetic acid and then used as the stabilizer to form AuNPs. The aminated Au PSNPs were then modified with PEG monomethyl ether with the other end of N-hydroxysuccinimidyl ester group (*m*PEG-NHS), followed by complete acetylation of the remaining PEI amines (Scheme 1b). The obtained Au PSNPs were characterized *via* different techniques. Hemolysis and cell viability assays were used to evaluate the hemocompatibility and cytocompatibility of the particles. Pharmacokinetic study was used to evaluate the half-decay time of the particles. The use of the Au PSNPs for CT imaging of blood pool and major organs of rats, lymph node of rabbits, and xenografted tumor model of mice was systematically carried out. Finally the *in vivo* biodistribution, stability, toxicity, and blood analysis of the particles were also thoroughly performed in order to elucidate the clinical potential to use the Au PSNPs as a CT contrast agent. To our knowledge, this is

the first report related to the development of ultrastable Au PSNPs formed using Au-S bond for CT imaging of different biological systems.

Experimental

Materials

Branched PEI (Mw = 25000), 1-ethyl-3-(3-(dimethylamino)propyl) carbodiimide hydrochloride (EDC), *N*-hydroxysuccinimide (NHS), mercaptoacetic acid, and 3-(4,5-dimethylthiazol-2-yl)-2,5-diphenyltetrazolium bromide (MTT) were supplied by Sigma-Aldrich (St. Luis, MO). *m*PEG-NHS (Mw =2000) was obtained from Shanghai Seebio Biotech, Inc. (Shanghai, China). Triethylamine (TEA), acetic anhydride (Ac$_2$O), HAuCl$_4$·4H$_2$O, and all the other chemicals were obtained from Sinopharm Chemical Reagent Co., Ltd. (Shanghai, China) and used without further purification. Roswell Park Memorial Institute-1640 (RPMI-1640) medium, Minimum Essential Medium (MEM), fetal bovine serum (FBS), penicillin, and streptomycin were obtained from HyClone Lab., Inc. KB cells (a human epithelial carcinoma cell line) and L929 cells (a mouse fibroblast cell line) were acquired from Institute of Biochemistry and Cell Biology, the Chinese Academy of Sciences (Shanghai, China). Water used in all experiments was purified using a Milli-Q Plus185 water purification system (Millipore, Bedford, MA) with resistivity higher than 18 MΩ cm. Regenerated cellulose dialysis membranes with molecular weight cut-off (MWCO) of 8 000-14000 and 100 000 were supplied by Shanghai Yuanye Biotechnology Co., Ltd (Shanghai, China).

Synthesis of thiolated PEI

Firstly, PEI (40.0 mg) was dissolved in 20 mL water. Mercaptoacetic acid (8.9 μL, 80 molar equiv. of PEI) dissolved in 5.0 mL water was activated by EDC/NHS (5 molar equiv. of mercaptoacetic acid, 122.7 mg EDC, and 64.0 mg NHS) under vigorous magnetic stirring for 2 h. Then, the activated mercaptoacetic acid was dropped into the above PEI solution under vigorous magnetic stirring. After 24 h, the reaction
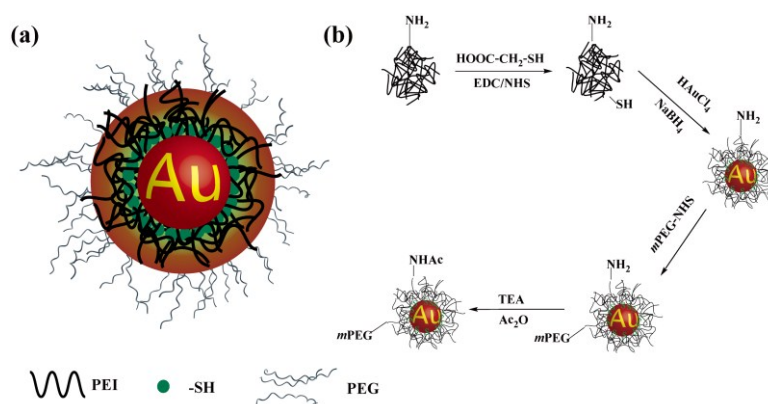
Scheme 1. Schematic illustration of the design (a) and synthesis procedure (b) of functional Au PSNPs for CT imaging applications.

mixture was dialyzed against phosphate buffered saline (PBS) and water for 3 days using a dialysis membrane with MWCO of 8000-14000, followed by lyophilization to obtain the thiolated PEI (PEI.NH$_2$-SH).

Synthesis of Au PSNPs

NaBH$_4$ reduction chemistry was used to prepare Au PSNPs with an Au salt/PEI.NH$_2$-SH molar ratio of 500:1. In brief, PEI.NH$_2$-SH (51.8 mg) dissolved in 20 mL water was added with an HAuCl$_4$ solution (27.2 mg/mL, 10 mL) and stirred for 10 min. Then, NaBH$_4$ (50 mg/mL in cool water, 3 mL) was rapidly added into the Au salt/PEI.NH$_2$-SH mixture solution under vigorous stirring. One hour later, mPEG-NHS (60.0 mg, 0.012 mmol, 5.0 mL in water) was added to the above mixture under stirring, and the reaction was stopped after 24 h. Finally, the remaining PEI amines were completely acetylated according to protocols reported in the literature[33] and the reaction mixture was purified and lyophilized according to the procedures used for the purification of PEI.NH$_2$-SH to get the {(Au^0)$_{500}$-PEI.NHAc-SH-mPEG} NPs (Au PSNPs).

Characterization techniques

^{1}H NMR spectra were recorded by a nuclear magnetic resonance spectrometer (Bruker DRX 400, Germany). UV-Vis spectroscopy was carried out using a PerkinElmer Lambda 25 spectrophotometer. The morphology of the Au PSNPs was characterized via transmission electron microscopy (TEM) imaging (2010F JEOL analytical electron microscope, Tokyo, Japan) with an operating voltage of 200 kV. The Au composition of the synthesized Au PSNPs was determined by inductively coupled plasma-optical emission spectroscopy (ICP-OES, Leeman Prodigy, Hudson, NH). Au PSNPs (1.9 mg) was digested by 10 mL aqua regia solution for 4 h, then 0.5 mL solution was taken and diluted with 4.5 mL water for ICP-OES analysis. According to the ICP-OES results, there were 1 μmol Au per 382 μg Au PSNPs. This Au content was used for the Au concentration determination in the following X-ray attenuation intensity, hemolysis, cytocompatibility, and in $vivo$ studies. The hydrodynamic size and zeta-potential of the particles were measured using a Zetasizer Nano ZS system (Malvern, UK) equipped with a standard 630 nm laser. In $vitro$ CT imaging and X-ray attenuation intensity measurements of samples were performed with a GE Light Speed VCT imaging system (GE Medical Systems, Milwaukee, WI) according to protocols reported in our previous work.[2] Aqueous solutions of iohexol 300 (Omnipaque) and the formed Au PSNPs with different I or Au molar concentrations (0.01, 0.02, 0.05, 0.075, and 0.1 M, respectively) were prepared and analyzed.

Hemolysis assay

Fresh human blood stabilized with citrate was provided by Shanghai General Hospital (Shanghai, China) and used after approval by the ethical committee of Shanghai General Hospital. Red blood cells (RBCs) were separated from fresh blood by centrifugation (3000 rpm, 3 min), washed with PBS for 4 times, and diluted 10 times with PBS.[39] After that, 0.1 mL of the diluted RBC suspension was mixed with 0.9 mL PBS (negative control), 0.9 mL water (positive control), or 0.9 mL PBS containing Au PSNPs with different final Au concentrations (50, 100, 200,400, and 800 μM, respectively). Meanwhile, 0.1 mL PBS added to 0.9 mL PBS containing Au PSNPs with the same concentrations were used as the blank controls. The mixtures were left to stand for 2 h and centrifuged at 10 000 rpm for 2 min. Finally, the absorbance at 541 nm of the supernatants was measured by UV-Vis spectrophotometer and the hemolysis percentages of the samples were calculated according to the following equation:

$$\text{Hemolysis percentage} = (A_s - A_{bc} - A_{nc})/(A_{pc} - A_{nc}) \times 100\% \quad (1)$$

where A_s is the absorbance value of the samples, A_{bc}, A_{nc}, and A_{pc} are the absorbance values of the blank, negative, and positive controls, respectively. Each experiment was performed in triplicate and the results were shown as mean ± standard deviation.

Cytocompatibility assay

The cytocompatibility of the formed Au PSNPs was quantified by MTT viability assay of KB and L929 cells. Briefly, KB or L929 cells were cultured in 96-well plates as a density of 8000 per well in a 37 °C incubator with 5% CO$_2$. After overnight incubation, the medium was replaced with the fresh RPMI 1640 or MEM cell culture medium containing Au PSNPs at the different Au molar concentrations (0, 10, 20, 40, 70, and 100 μM, respectively). After 24 h, MTT solution (20 μL in PBS, 5 mg/mL) was added to each well and the cell viability was measured at 570 nm using a Thermo Scientific Multiskan MK3 ELISA reader (Waltham, MA). Each experiment was performed in triplicate, and the results were shown as mean ± standard deviation.

Pharmacokinetics

Animal experiments were carried out according to protocols approved by the institutional committee for animal care. Six animals were used as a group in each in $vivo$ experiment. For pharmacokinetic study, an Au PSNP saline solution (0.15 mL, [Au] = 0.1 M) was intravenously injected through the tail vein of Blab/c mice (22-26 g, Shanghai Slac Laboratory Animal Center, Shanghai, China). The blood was harvested from eyeball of mice at different time points postinjection (0.5, 1, 2, 4, 8, 12, 24, and 36 h, respectively). Then, the collected blood samples were carefully weighed and digested by 1 mL aqua regia solution overnight. After diluted with 2 mL water, the Au content in the samples was measured by ICP-OES.

CT imaging of blood pool and major organs of rats

For in $vivo$ blood pool CT imaging, Sprague–Dawley (SD) rats (180–210 g, Sino-British SIPPR/BK Lab Animal Ltd., Shanghai, China) were firstly anesthetized through intraperitoneal administration of pentobarbital sodium (40 mg/kg). Subsequently, a saline solution of Au PSNPs (1.0 mL, [Au] = 0.1 M) was intravenously injected through the tail vein (n = 6). CT images were obtained before and after administration of the

materials at different time points (1, 4, and 24h, respectively) using a GE LightSpeed VCT clinical imaging system with a tube voltage of 100 kV, an electrical current of 220 mA, and a slice thickness of 1.25 mm. Reconstructed 3D images were obtained using the GE Advantage Workstation AW4.4.

CT imaging of lymph node of rabbits

For lymph node CT imaging, about 1.5 kg male New Zealand white rabbits (Sino-British SIPPR/BK Lab Animal Ltd., Shanghai, China) were anesthetized by intraperitoneal injection of pentobarbital sodium (40 mg/kg). Subsequently, 0.50 mL Au PSNPs ([Au] = 0.1 M) saline solution was injected intradermally into the left paw of the rabbits (n = 6). Meanwhile, the right paw of the rabbit was administrated with 0.5 mL saline solution as control. CT scans were performed 4 h after administration using the same instrument and parameter with that in blood pool imaging.

CT imaging of a xenografted tumor model

Male BALB/c nude mice (20-25 g, Shanghai Slac Laboratory Animal Center) were subcutaneously injected with 5×10^6 KB cells in 0.1 mL PBS solution on the right side of their flanks. While the tumor nodules reached a volume of 0.2-0.4 cm^3, Au PSNPs ([Au] = 0.1 M, in 0.15 mL PBS) were intravenously injected *via* the tail vein. CT images were acquired before and at 2, 4, and 6 h postinjection. The CT images were processed on a micro-CT imaging system with voxel $45 \times 45 \times 45$ μm and display field of view of 10-25 mm. CT values were obtained using the software supplied by the manufacturer.

In vivo biodistribution and stability

For *in vivo* biodistribution studies, Au PSNPs ([Au] = 0.1 M, 0.15 mL in saline) were intravenously injected through the tail vein to the Balb/c mice. Then, the mice (n = 6) were sacrificed at different time points postinjection (1, 6, 24, 48, 96, and 192 h, respectively). Major organs (heart, liver, spleen, lung, and kidney) were carefully harvested, weighed, and digested by 2 mL aqua regia solution overnight. For the excretion study, feces and urine (about 0.15 g) were collected from mice (*n* = 6) at different time points postinjection (1, 2, 4, 8, 24, and 48 h, respectively). After carefully weighed and digested by aqua regia solution overnight, these samples were eroded to determine the Au contents in order to study the clearance of the particles. In addition, for *in vivo* stability studies, the particles found in urine were also isolated through dialysis against water using regenerated cellulose dialysis membranes with MWCO of 100 000 and subjected to TEM observation according to protocols described above.

In vivo toxicity studies

For *in vivo* toxicity studies, Balb/c mice (20-25 g) were intravenously administrated with Au PSNPs ([Au] = 0.1 M, 0.15 mL in saline) *via* the tail vein. Mice treated with 0.15 mL saline solution were used as control (n = 6 for each group). The body weight of Balb/c mice both in the experimental and control

groups was recorded over a time period of one month postinjection.

For histology studies, the above Balb/c mice were euthanized and their major organs were harvested. Then, the obtained organs were fixed in 10% formalin, embedded in paraffin, and sectioned with a thickness of 4 μm. Subsequently, the sections of organ samples were subjected to hematoxylin and eosin (H&E) staining and observed by an inverted phase contrast microscope (Leica DM IL LED).

Blood analysis

For serum biochemistry assays, healthy Balb/c mice (n = 6) were intravenously injected with Au PSNPs ([Au] = 0.1 M, 0.15 mL in saline, for each mouse) through the tail vein. The control mice (n = 6) were injected with saline (0.15 mL for each mouse). The blood of each mouse was harvested from eyeball one month post administration. Blood supernatant was obtained by centrifugation and used to analyze the serum biochemistry parameters including ALT (alanine aminotransferase), ALP (alkaline phosphatase), AST (aspartate aminotransferase), BUN (blood urea nitrogen), TP (total protein), CREA (creatinine), GLOB (globulin), as well as TBIL (total bilirubin). The rest of blood was used for routine blood test including RBC, WBC (white blood cell), PLT (platelet), HGB (hemoglobin), HCT (hematocrit), MCV (mean corpuscular volume), MCHC (mean corpuscular hemoglobin concentration), and MCH (mean corpuscular hemoglobin).

Statistical analysis

One way ANOVA statistical analysis was carried out to evaluate the significance of all the obtained experimental data, and 0.05 was selected as the significance level.

Results and discussion

Synthesis and characterization of Au PSNPs

To prove our hypothesis that thiolated PEI is able to be used as a stabilizer to synthesize AuNPs with ultrastability for CT imaging applications, we first synthesized thiolated PEI (PEI.NH$_2$-SH), used the PEI-SH to synthesize Au PSNPs, followed by sequential PEI amine-enabled PEGylation modification of the particles and acetylation of the remaining PEI surface amines (Scheme 1).

PEI was first covalently modified with mercaptoacetic acid *via* EDC chemistry, and the formed PEI.NH$_2$-SH was characterized by ^{1}H NMR spectroscopy (Figure S1b, Supporting Information). It can be seen that there are two main peaks at 2.5 and 3.2 ppm, respectively, whereas the pristine PEI only displays the methylene proton signals at 2.5 ppm (Figure S1a). The new peak at about 3.2 ppm is related to the -CH$_2$- proton signals of PEI linked with the secondary and tertiary amides,[32] while the chemical shift at 2.5 ppm is associated with the -CH$_2$- proton signals of PEI linked with the tertiary and unreacted PEI primary and secondary amines. These results were consistent with those reported in the literature.[32, 40] The number of SH per PEI amine was calculated to be 15% based on three

batches of PEI.NH$_2$-SH, which is slightly less than the calculated value of 20% based on the initial molar feeding ratio of mercaptoacetic acid and PEI amine. In addition, zeta potential of PEI and PEI.NH$_2$-SH was tested to confirm the surface modification (Table S1, Supporting Information). It is clear that the positive surface potential of PEI (45.32 ± 5.15 mV) decreased to 34.17 ± 6.21 mV after the modification of mercaptoacetic acid.

Thiolated PEG shows its advantages as the steric stabilizer and antifouling spacer for AuNPs under complicated conditions.[41, 42] Therefore, for better *in vivo* biomedical applications, it is essential to further modify the amine functionality of the Au PSNPs *via* PEGylation to improve the biocompatibility and increase the circulating time of the particles.[43-45] As shown in Figure S1c, compared with the ^{1}H NMR spectrum of the PEI.NH$_2$-SH, {(Au^0)$_{500}$-PEI.NH$_2$-SH-*m*PEG} NPs show additional peaks at 3.5 and 3.2 ppm, relating to ethylene back bone and methoxyl protons of PEG, respectively. The number of *m*PEG per PEI was calculated to be 19.1, approximately equal to the initial molar feeding ratio. The PEGylation modification was also confirmed by zeta potential measurements, where the surface potential of the {(Au^0)$_{500}$-PEI.NH$_2$-SH-*m*PEG} NPs (18.42 ± 3.45 mV) significantly decreases when compared with that of the PEI.NH$_2$-SH (Table S1). To further reduce the surface positive potential of the particles, the remaining PEI amines of the {(Au^0)$_{500}$-PEI.NH$_2$-SH-*m*PEG} NPs were further acetylated, leading to the formation of the final Au PSNPs with a slight positive potential (1.78 ± 0.94 mV, Table S1). This is believed to render the particles with prolonged circulation time and reduced long-term toxicity.

The resulting Au PSNPs were then characterized by UV-Vis spectrometry and TEM imaging. As shown in the UV-Vis spectrum (Figure 1a), the prominent surface plasma resonance (SPR) peak at 521 nm clearly indicates the formation of AuNPs. TEM imaging shows that the formed Au PSNPs have a spherical shape (Figure 1b) with a mean diameter of 5.1 nm and a relatively uniform size distribution (Figure 1c). This suggests that PEI.NH$_2$-SH is effective to restrict the growth of AuNPs *via* Au-S bond formation to form uniform NPs. The hydrodynamic size of the Au PSNPs dispersed in water was measured to be 64.8 ± 3.6 nm with the polydispersity index of 0.18 by dynamic light scattering (DLS), which is much larger than that measured by TEM (Figure S2a, Supporting Information). This is due to the fact that DLS measures particles in a hydrated state, which may form clustered structure consisting of many Au PSNPs, while TEM only measures the single metal core NPs. The large-area TEM image of the NPs (Figure S2b, Supporting Information) clearly shows the clustered structure of the formed nanoparticles instead of aggregation in hydrated state. The number of Au atom per PEI was measured to be 487 ± 11 by ICP-OES, which is quite consistent with the initial molar feeding ratio (500).

Stability of Au PSNPs

The stability of the colloidal NPs is a key factor for their applications in CT imaging. Thus, the stability of the Au PSNPs under different temperature and pH conditions was monitored by UV-Vis spectrometry.[22] The results reveal that the absorption features of Au PSNPs do not display any appreciable changes in the pH range of 4.0-8.0 (10 mM acetic buffer for pH 4.0 and 5.0; 10 mM PBS for pH 7.0 and 8.0) and the temperatures of 4-50 °C (Figure S3, Supporting Information), suggesting the good stability of the formed Au PSNPs in the given pH and temperature range. It is notable that the {(Au^0)$_{500}$-PEI.NHAc-*m*PEG} NPs formed according to our previous work[33] without the SH modifications started to aggregate within one week (Figure S4, Supporting Information). Moreover, the colloidal stability of the formed Au PSNPs was further monitored by measuring their hydrodynamic size in both PBS solution and cell medium, which does not show any appreciable changes for at least 1 week (Figure S5, Supporting Information). This results was different with the previous report[46] that the bonding mode of thiolated DNA and gold changes with pH and temperature. This is because the thiolated PEI containing more than 100 SH, which could effectively protect the Au nanoparticles and did not sensitive to the condition changes. Taken together, our results suggest that the formed Au PSNPs are quite stable, which is beneficial for their further *in vivo* applications.

X-ray attenuation property

To explore the potential to use the developed Au PSNPs for CT
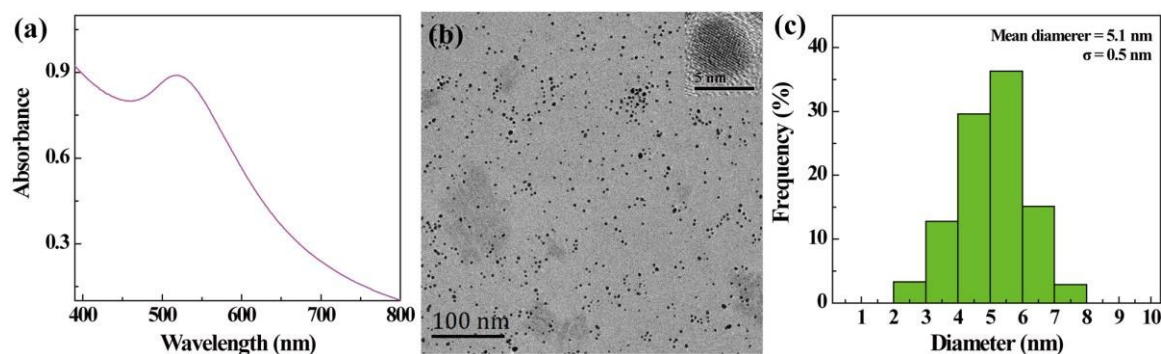
Figure 1. UV-Vis spectrum (a), TEM image (b), and size distribution histogram (c) of the formed Au PSNPs. The inset shows the high-resolution TEM image of the Au PSNPs.
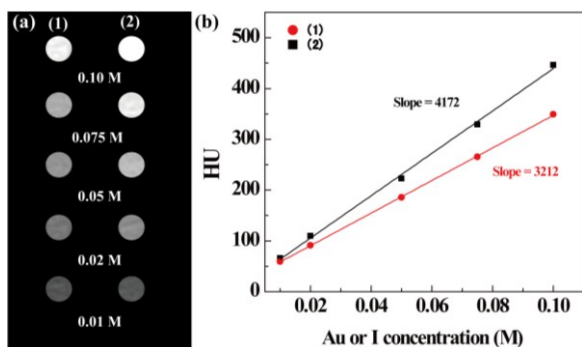
Figure 2. CT images (a) and linear fitting (b) of Omnipaque (1) and Au PSNPs (2) as a function of I or Au molar concentration.
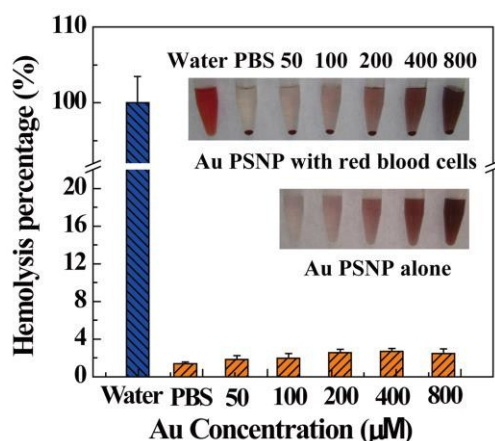
Figure 3. Hemolytical activity of the Au PSNPs at different concentrations (50, 100, 200, 400, and 800 μM, respectively). Water and PBS were used as positive and negative control, respectively. The insets show the photograph of centrifuged red blood cells after exposed to water, PBS, and PBS containing different concentrations of the Au PSNPs, and the suspension of Au PSNPs alone with the corresponding concentrations.

Figure 4. MTT assay of the viability of KB and L929 cells after treatment with Au PSNPs at the Au concentrations of 0-100 μM for 24 h (a), and blood circulation and pharmacokinetic data obtained for the Au PSNPs (b).

imaging applications, CT phantom studies of the particles and Omnipaque were first performed (Figure 2). Au PSNPs and Omnipaque with the same concentrations of radiodense element (Au or I) were analyzed (Figure 2a). It can be seen that the attenuation intensity of both Au PSNPs and Omnipaque increases with the Au or I concentration. Under the same radiodense element concentrations, the attenuation intensity of Au PSNPs is higher than that of Omnipaque (Figure 2b). The slope of the HU value of Au PSNPs (4172) as a function of Au concentration is higher than that of the Omnipaque (3212) as a function of iodine concentration (Figure 2b). This better X-ray attenuation property of Au PSNPs than that of Omnipaque should be due to the relatively higher K-edge energy of Au (80.7 KeV) than that of iodine (33.2 keV).[18] Therefore, the formed Au PSNPs should have a great potential for enhanced CT imaging applications.

Hemolysis assay

For *in vivo* CT imaging applications, it is important to assess the hemocompatibility of the developed Au PSNPs. In this study,

the hemocompatibility of Au PSNPs was preliminarily evaluated by hemolysis assay (Figure 3). Apparently, the Au PSNPs do not display any hemolytic activity at the Au concentration up to 800 μM, similar to the negative PBS control. In contrast, the HRBCs exposed to water (positive control) display obvious hemolysis effect (Figure 3, inset). The hemolysis percentage of the Au PSNPs was further quantified *via* UV-Vis spectroscopic measurement of the absorption of hemoglobin in the supernatant. We show that the hemolysis percentages of Au PSNPs at the Au concentration up to 800 μM are all less than 3.0%, indicating their non-hemolytic behavior in the given concentration range.

***In vitro* cytotoxicity assay**

Before application of the formed Au PSNPs as a contrast agent for *in vivo* CT imaging, the cytocompatibility of the materials was tested *via* MTT viability assay of the cancer cells (KB cells) and the normal cells (L929 cells). As shown in figure 4a, the viability of both KB and L929 cells treated with the Au PSNPs does not have any appreciable changes at the Au concentration up to 100 μM when compared with the control cells treated with PBS. This suggests that the developed Au PSNPs with PEI amines modified with PEGylation and acetylation are cytocompatible at the Au concentration up to 100 μM.

Pharmacokinetics

For blood pool CT imaging, it is important to investigate the pharmacokinetics of the formed Au PSNPs. The Au content in
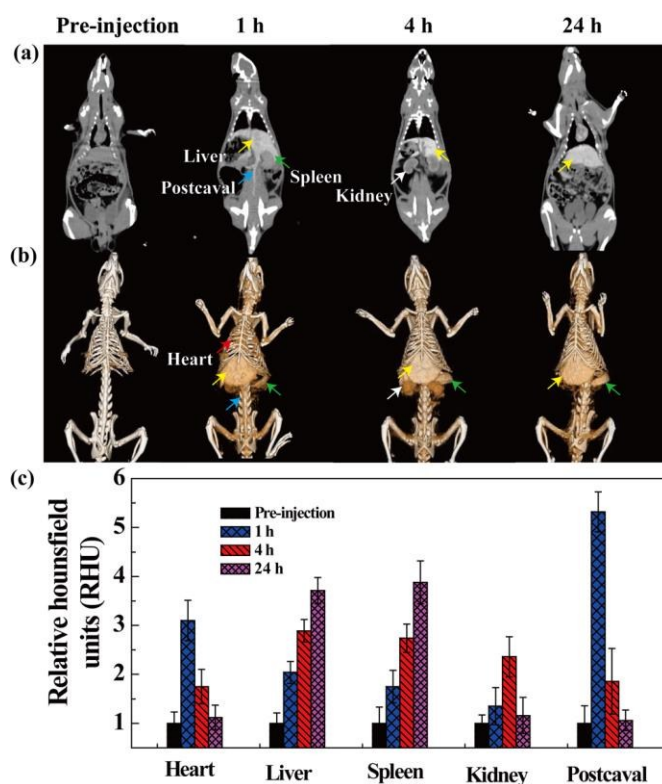
Figure 5. CT images of a mouse postcaval vein, heart, liver, spleen, and kidney after intravenous injection of the Au PSNPs at different time points postinjection (a), the corresponding 3D renderings of the *in vivo* CT images (b), and the relative CT enhancement of the postcaval vein, heart, liver, spleen, and kidney (c).

the blood of mice at different time points postinjection was determined by ICP-OES (Figure 4b). The half-decay time of the Au PSNPs was calculated to be 7.8 h, which is comparable to that of PEGylated PEI-entrapped AuNPs reported in our previous work.[33] The relatively long blood circulation time of the Au PSNPs could be due to the surface PEGylation-induced antifouling property of the particles,[45] which is amenable for their further applications in blood pool and tumor CT imaging.

Blood pool and organ CT imaging

The encouraging X-ray attenuation property and relatively long blood circulation time of the Au PSNPs prompted us to explore their potential for blood pool and organ CT imaging. In general, only the bone region appears to be bright in the CT image because of their strong X-ray absorption property, while the blood vessels cannot be differentiated from other soft tissues. As shown in figure 5a, the postcaval vein can be clearly observed even at 1 h postinjection, indicating the long circulation time and enhanced CT contrast enhancement of the formed Au PSNPs. While the postcaval vein appears to be darker with the time postinjection, the liver and spleen regions become brighter with time, due to the accumulation of the particles by macrophages in the liver and spleen. In the reconstructed 3D CT images (Figure 5b and Figure S6, Supporting Information), the heart, liver, spleen, kidney, and postcaval vein can be clearly observed at different time points postinjection. For quantitative analysis of the CT contrast enhancement, the average HU of interest regions was

measured and the relative HU (RHU) was calculated as the ratio of the HU in the post-administration image and the pre-administration image (Figure 5c). The RHU values of the postcaval vein and heart reduce gradually from 5.4 and 3.0 to 1.0 and 1.1, respectively from 1 h to 24 h postinjection, while the RHU values of the liver and spleen rapidly increase from around 2.0 to 4.0 from 1 h to 24 h postinjection. These results indicate that the formed Au PSNPs have a great potential to be used as a contrast agent for blood pool and organ CT imaging.

Lymph node CT imaging

We next explored the feasibility to use the Au PSNPs for lymph node CT imaging. The lymphatic system is a common route for cancer metastasis.[15] However, the clinically used blue dyes suffer from short imaging time, limiting their usage for cancer metastasis detection.[47] In CT image of a rabbit before injection,
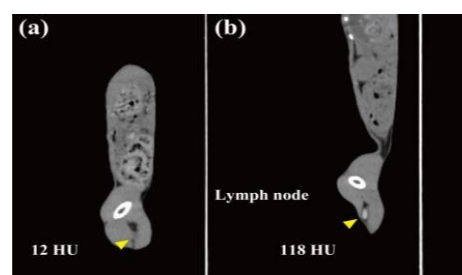
Figure 6. CT images and CT value of a rabbit lymph node before and at 3 h post hock injection of the Au PSNPs.

lymph-node area has little inherent contrast when
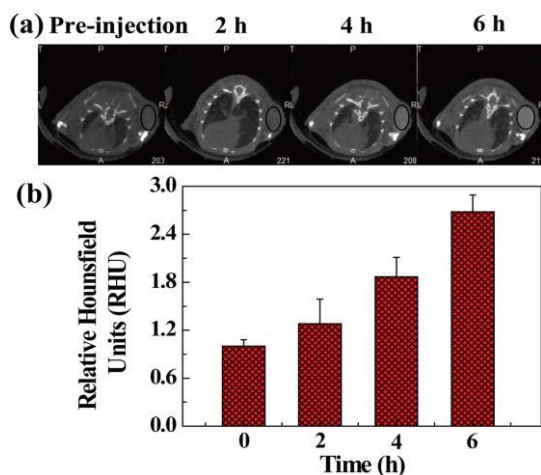
Figure 7. CT images (a) and the relative CT enhancement (b) of the xenografts KB tumor model before and at different time points post intravenous injection of the Au PSNPs.

compared with the surrounding muscle (Figure 6a). However, upon subcutaneous injection of Au PSNPs into the footpad of a normal rabbit, their accumulation in the popliteal lymph node could be clearly seen at 3 h postinjection (Figure 6b). This suggests that the efficient diffusion of the Au PSNPs to the lymph-node area from the injection part. Quantitatively, the HU value of the lymph node region increased significantly from 12.0 ± 1.7 to 118.0 ± 8.6, and the RHU values of the lymph node increased from 0.9 ± 0.1 to 8.8 ± 0.7. The excellent lymph node CT imaging performance of the Au PSNPs could be used to precisely detect cancer metastasis by lymph node mapping.

In vivo tumor model CT imaging

With the long circulation time and excellent *in vivo* blood pool and major organ CT imaging performance of Au PSNPs, we next pursued their applicability for *in vivo* tumor CT imaging (Figure 7). It is clear that before administration of the Au PSNPs, there is almost no inherent contrast between tumor and surrounding muscle in the CT image (Figure 7a). However, the tumor site displays much more CT contrast enhancement at different time points postinjection of the Au PSNPs. Moreover, the CT contrast enhancement of the tumor lesion gradually improves with the time postinjection and the tumor CT image is getting sharper with clear tumor boundary. This suggests that the injected Au PSNPs are able to be gradually accumulated to the tumor region *via* the known enhanced permeability and retention (EPR) effect, allowing for effective tumor CT imaging. The RHU of the tumor region was also quantified, and the value increased steadily and reached 192± 13.6% at 6 h postinjection (Figure 7b). Our results demonstrated that the developed Au PSNPs are able to be used as a contrast agent for effective tumor CT imaging *via* a passive EPR effect.

In vivo biodistribution and stability study
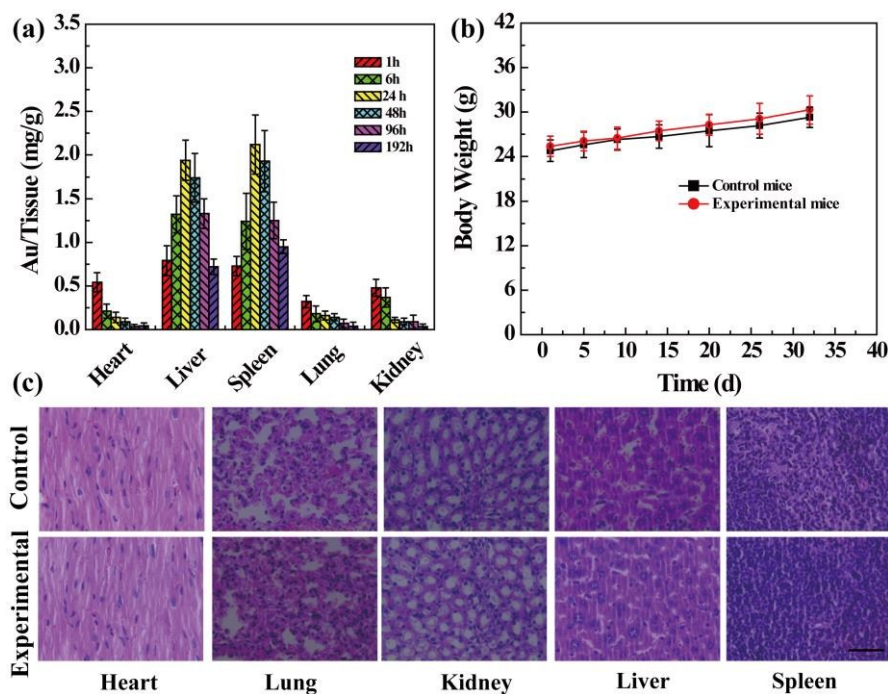
Figure 8. Biodistribution of the Au PSNPs in the major organs of the mice at different time points postinjection (a), changes in body weight of mice injected with saline (control group) and Au PSNPs (experimental group) (b), and histological changes of the mouse organs stained with H&E at 32 days postinjection (c).The scale bar in (c) represents 50 μm.

To investigate the biodistribution of the Au PSNPs in mice at different time points postinjection, the major organs (heart, liver, spleen, lung, and kidney) of the tested mice were collected and the Au uptake was quantified by ICP-OES (Figure 8a). It can be seen that at 1 h postinjection, all the studied organs have a quite low Au uptake with 0.54, 0.79, 0.73, 0.32, and 0.48 mg/g tissue for the heart, liver, spleen, lung, and kidney, respectively. This is due to fact that the formed Au PSNPs have a relatively long half-decay time (7.8 h) as demonstrated by pharmacokinetic studies. With the time postinjection, liver and spleen show the increased Au uptake, while other three organs have reduced Au uptake. This suggests that the Au PSNPs could be cleared from blood with the time postinjection and taken up by the liver and spleen with a peak Au uptake at 24 h postinjection. Importantly, the Au uptake in both liver and spleen shows a gradual decrease at 48 h postinjection (with about 1.74 mg/g and 1.93 mg/g in the liver and spleen, respectively), and have only 0.72 and 0.95 mg/g Au uptake in the liver and spleen, respectively at 192 h postinjection. This indicates that the Au PSNPs are able to gradually clear out of body. These results suggest that the Au PSNPs are quite biocompatible and do not introduce apparent *in vivo* toxicity.

To further disclose the elimination route of the Au PSNPs, urine and feces samples were collected at different time points postinjection, and the Au content of these samples were quantified according to the protocols described in the literature.[48] As shown in figure S7 (Supporting Information), Au PSNPs can be detected in the samples of both feces and urine,

suggesting that the particle clearance pathway may be through both renal and fecal excretions.

The stability of the Au PSNPs is a key factor for their applications in CT imaging. Apart from the *in vitro* stability evaluation, the *in vivo* stability of the Au PSNPs was also studied. The urine sample collected on the second day post administration was purified and subjected to TEM analysis to confirm the shape and size of the Au PSNPs excreted in the urine (Figure S8, Supporting Information). It is clear that the average size of Au PSNPs is 5.2 ± 0.7 nm, which is quite similar to that of the NPs before administration (Figure 1), further confirming the excellent stability of the developed Au PSNPs synthesized via the Au-S bond formation.

Toxicology investigation

To explore the clinical aspects or potential to use the Au PSNPs for CT imaging applications, long-term *in vivo* toxicity of the Au PSNPs was systematically evaluated *via* the monitoring the body weight, analysis of serum biochemistry parameters, as well as observation of the histological changes of the major organs after the administration of Au PSNPs into mice. As shown in figure 8b, mice injected with the Au PSNPs display a trend in the body weight changes similar to the control mice treat with saline over a 32-day time period. In addition, the H&E stained slices of the major organs (heart, lung, kidney, liver, and spleen) of mice injected with the Au PSNPs (experimental group) do not show any perceptible lesions, hydropic damages, and any other adverse effect compared with that of the control group injection with saline at 32 days postinjection (Figure 8c). Our bio-safety results show that the developed Au PSNPs display excellent biocompatibility *in vivo*.

For the hematological assessment, we also selected standard hematology markers to analyze the blood compatibility of the Au PSNPs including the WBC, RBC, PLT, HCT, MCV, MCH, HGB, and MCHC. As shown in Figure 9a, all the 8 parameters in mice treated with the Au PSNPs do not have any significant difference from those in the control mice, and are all in the normal range. This indicates that the Au PSNPs do not show any appreciable toxicity to the mice. Furthermore, all biochemical parameters of the experimental group are approximately similar to those of the control group (Figure 9b). It is notable that the normal liver function parameters including AST, ALP and ALT could prove the hepatic safety of the injected Au PSNPs. Also, CREA and BUN are the main indicators of renal function, and the measured normal values indicate the good function of kidney and renal safety of the Au PSNPs. Taken together, our results show that there is no obvious hepatic and renal toxicity observed after Au PSNPs were injected into mice.
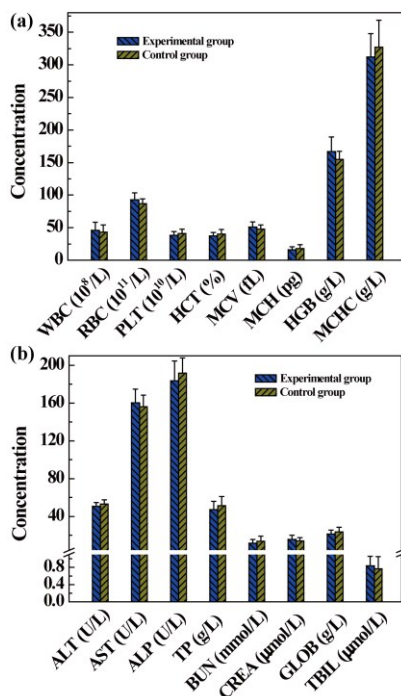
Figure 9. Hematology data (a) and blood biochemistry data (b) of the mice treated with saline (control group) and the Au PSNPs (experimental group).

Conclusions

In summary, a facile approach has been developed to synthesize ultrastable Au PSNPs for CT imaging applications. By using thiolated PEI as a stabilizer and the subsequent PEI amine-enabled PEGylation and acetylation functionalization of

the particles, ultrastable Au PSNPs with an Au core size of 5.1 nm and half-decay time of 7.8 h can be formed. The Au PSNPs possess good hemocompatibility, cytocompatibility, and *in vivo* organ and blood biocompatibility, and are able to be used as a contrast agent for blood pool, major organ, lymph node, and tumor CT imaging. Our results suggest that the constructed Au PSNPs may be used as a versatile contrast agent for CT imaging of various biological systems. Moreover, with the high density of PEI amine groups, the strategy may be extended to construct targeted Au PSNP-based nanoprobes for targeted CT imaging of different diseases, in particular cancer.

Acknowledgements

Notes and references

1. H. Lusic and M. W. Grinstaff, *Chem. Rev.*, 2012, **113**, 1641-1666.
2. C. Peng, L. Zheng, Q. Chen, M. Shen, R. Guo, H. Wang, X. Cao, G. Zhang and X. Shi, *Biomaterials*, 2012, **33**, 1107-1119.
3. H. Xing, W. Bu, S. Zhang, X. Zheng, M. Li, F. Chen, Q. He, L. Zhou, W. Peng, Y. Hua and J. Shi, *Biomaterials*, 2012, **33**, 1079-1089.
4. A. Jakhmola, N. Anton and T. F. Vandamme, *Adv. Healthcare Mater.*, 2012, **1**, 413-431.
5. Y. Liu, K. Ai, J. Liu, Q. Yuan, Y. He and L. Lu, *Angew. Chem. Int. Ed.*, 2012, **51**, 1437-1442.
6. Q. Yin, F. Y. Yap, L. Yin, L. Ma, Q. Zhou, L. W. Dobrucki, T. M. Fan, R. C. Gaba and J. Cheng, *J. Am. Chem. Soc.*, 2013, **135**, 13620-13623.
7. Z. Liu, Z. Li, J. Liu, S. Gu, Q. Yuan, J. Ren and X. Qu, *Biomaterials*, 2012, **33**, 6748-6757.
8. O. Betzer, A. Shwartz, M. Motiei, G. Kazimirsky, I. Gispan, E. Damti, C. Brodie, G. Yadid and R. Popovtzer, *ACS Nano*, 2014, **8**, 9274-9285.
9. O. Rabin, J. Manuel Perez, J. Grimm, G. Wojtkiewicz and R. Weissleder, *Nat. Mater.*, 2006, **5**, 118-122.
10. F. Hyafil, J.-C. Cornily, J. E. Feig, R. Gordon, E. Vucic, V. Amirbekian, E. A. Fisher, V. Fuster, L. J. Feldman and Z. A. Fayad, *Nat. Med.*, 2007, **13**, 636-641.
11. E. Samei, R. S. Saunders, C. T. Badea, K. B. Ghaghada, L. W. Hedlund, Y. Qi, H. Yuan, R. C. Bentley and S. Mukundan Jr, *Int. J. Nanomed.*, 2009, **4**, 277.
12. E. Karathanasis, L. Chan, S. R. Balusu, C. J. D'Orsi, A. V. Annapragada, I. Sechopoulos and R. V. Bellamkonda, *Biomaterials*, 2008, **29**, 4815-4822.
13. V. P. Torchilin, *Adv. Drug Delivery Rev.*, 2002, **54**, 235-252.
14. S. Wen, K. Li, H. Cai, Q. Chen, M. Shen, Y. Huang, C. Peng, W. Hou, M. Zhu, G. Zhang and X. Shi, *Biomaterials*, 2013, **34**, 1570-1580.
15. M. H. Oh, N. Lee, H. Kim, S. P. Park, Y. Piao, J. Lee, S. W. Jun, W. K. Moon, S. H. Choi and T. Hyeon, *J. Am. Chem. Soc.*, 2011, **133**, 5508-5515.
16. Y. Liu, K. Ai and L. Lu, *Acc. Chem. Res.*, 2012, **45**, 1817-1827.
17. J. F. Hainfeld, D. N. Slatkin and H. M. Smilowitz, *Phys. Med. Biol.*, 2004, **49**, N309.
18. J. F. Hainfeld, D. N. Slatkin, T. M. Focella and H. M. Smilowitz, *Br. J. Radiol.*, 2006, **79**, 248-253.
19. S. Rana, A. Bajaj, R. Mout and V. M. Rotello, *Adv. Drug Delivery Rev.*, 2012, **64**, 200-216.
20. P. Ghosh, G. Han, M. De, C. K. Kim and V. M. Rotello, *Adv. Drug Delivery Rev.*, 2008, **60**, 1307-1315.
21. X. Shi, H. Gong, Y. Li, C. Wang, L. Cheng and Z. Liu, *Biomaterials*, 2013, **34**, 4786-4793.
22. S. Wen, F. Zheng, M. Shen and X. Shi, *Colloid Surf. A*, 2013, **419**, 80-86.
23. H. Cai, X. An, J. Cui, J. Li, S. Wen, K. Li, M. Shen, L. Zheng, G. Zhang and X. Shi, *ACS Appl. Mater. Interfaces*, 2013, **5**, 1722-1731.
24. C. Subramani, Y. Ofir, D. Patra, B. J. Jordan, I. W. Moran, M.-H. Park, K. R. Carter and V. M. Rotello, *Adv. Funct. Mater.*, 2009, **19**, 2937-2942.
25. Y. Zhu, G.-P. Tang and F.-J. Xu, *ACS Appl. Mater. Interfaces*, 2013, **5**, 1840-1848.
26. S. Wen, Q. Zhao, X. An, J. Zhu, W. Hou, K. Li, Y. Huang, M. Shen, W. Zhu and X. Shi, *Adv. Healthcare Mater.*, 2014, **3**, 1568-1577.
27. S. Shi, K. Shi, L. Tan, Y. Qu, G. Shen, B. Chu, S. Zhang, X. Su, X. Li, Y. Wei and Z. Qian, *Biomaterials*, 2014, **35**, 4536-4547.
28. D. Cheng, N. Cao, J. Chen, X. Yu and X. Shuai, *Biomaterials*, 2012, **33**, 1170-1179.
29. L. Y. Qiu and Y. H. Bae, *Biomaterials*, 2007, **28**, 4132-4142.
30. E. Wagner and J. Kloeckner, *Adv. Polym. Sci.*, 2006, **192**, 135-173.
31. A. C. Hunter, *Adv. Drug Delivery Rev.*, 2006, **58**, 1523-1531.
32. S. Wen, F. Zheng, M. Shen and X. Shi, *J. Appl. Polym. Sci.*, 2013, **128**, 3807-3813.
33. B. Zhou, L. Zheng, C. Peng, D. Li, J. Li, S. Wen, M. Shen, G. Zhang and X. Shi, *ACS Appl. Mater. Interfaces*, 2014, **6**, 17190-17199.
34. D. Li, S. Wen and X. Shi, *Wiley Interdiscip. Rev.: Nanomed. Nanobiotechnol.*, 2015, DOI: 10.1002/wnan.1331, DOI: 10.1002/wnan.1331.
35. E. Pensa, E. Cortés, G. Corthey, P. Carro, C. Vericat, M. H. Fonticelli, G. Benítez, A. A. Rubert and R. C. Salvarezza, *Acc. Chem. Res.*, 2012, **45**, 1183-1192.
36. W.-J. Song, J.-Z. Du, T.-M. Sun, P.-Z. Zhang and J. Wang, *Small*, 2010, **6**, 239-246.
37. M. Thomas and A. M. Klibanov, *Proc. Natl. Acad. Sci. USA*, 2003, **100**, 9138-9143.
38. A. Sharma, A. Tandon, J. C. K. Tovey, R. Gupta, J. D. Robertson, J. A. Fortune, A. M. Klibanov, J. W. Cowden, F. G. Rieger and R. R. Mohan, *Nanomedicine: Nanotechnology, Biology and Medicine*, 2011, **7**, 505-513.

Nanoscale Accepted Manuscript

39. S. Wang, S. Wen, M. Shen, R. Guo, X. Cao, J. Wang and X. Shi, *Int. J. Nanomed.*, 2011, **6**, 3449.
40. N. P. Gabrielson and D. W. Pack, *Biomacromolecules*, 2006, **7**, 2427-2435.
41. K. Siriwardana, M. Gadogbe, S. M. Ansar, E. S. Vasquez, W. E. Collier, S. Zou, K. B. Walters and D. Zhang, *J. Phys. Chem. C*, 2014, **118**, 11111-11119.
42. W. Wang, Q.-Q. Wei, J. Wang, B.-C. Wang, S.-h. Zhang and Z. Yuan, *J. Colloid. Surf. Sci.*, 2013, **404**, 223-229.
43. J. V. Jokerst, T. Lobovkina, R. N. Zare and S. S. Gambhir, *Nanomedicine*, 2011, **6**, 715-728.
44. M. Roberts, M. Bentley and J. Harris, *Adv. Drug Delivery Rev.*, 2012, **64**, 116-127.
45. D. Kim, S. Park, J. H. Lee, Y. Y. Jeong and S. Jon, *J. Am. Chem. Soc.*, 2007, **129**, 7661-7665.
46. N. Bhatt, P.-J. J. Huang, N. Dave and J. Liu, *Langmuir*, 2011, **27**, 6132-6137.
47. M. A. Swartz and A. W. Lund, *Nat. Rev. Cancer*, 2012, **12**, 210-219.
48. H. Wu, G. Liu, Y. Zhuang, D. Wu, H. Zhang, H. Yang, H. Hu and S. Yang, *Biomaterials*, 2011, **32**, 4867-4876.

Nanoscale Accepted Manuscript